Contribution from the Anorganisch Chemisch Laboratorium and Laboratorium voor Kristallografie, Universiteit van Amsterdam, J. H. van't Hoff Instituut, Nieuwe Achtergracht 166, 1018 WV Amsterdam, The Netherlands

Metal to Ligand Charge-Transfer Photochemistry of Metal–Metal-Bonded Complexes. 8.† Photochemistry of $(CO)_5MnMn(CO)_3(\alpha$-diimine) Complexes. Coupling Reactions of the Radicals Formed and X-ray Structure of the Photoproduct $(CO)_4Mn(\sigma$-*N*,σ-*N*′,η^2-*CN*-iPr-pyca)$Mn(CO)_3$

Tim van der Graaf,‡,‖ Derk J. Stufkens,*,‡ Ad Oskam,‡ and Kees Goubitz§

Received April 4, 1990

This article describes the photochemistry between 133 and 298 K of five metal–metal-bonded carbonyls $(CO)_5MnMn(CO)_3(\alpha$-diimine) (**1a–e**) (α-diimine = 4,4′-dimethyl-2,2′-bipyridine (bpy′ (**1a**)), pyridine-2-carbaldehyde *N*-isopropylimine (iPr-pyca (**1b**)), 1,4-diisopropyl-1,4-diaza-1,3-butadiene (iPr-DAB (**1c**)), 1,4-di-*p*-tolyl-1,4-diaza-1,3-butadiene (pTol-DAB (**1d**)), 1,4-di-*p*-anisyl-1,4-diaza-1,3-butadiene (pAn-DAB (**1e**))) by irradiation into their metal to α-diimine charge-transfer (MLCT) band. At room temperature these complexes undergo homolysis of the metal–metal bond and the radicals formed dimerize to give $Mn_2(CO)_{10}$ and $Mn_2(CO)_6(\alpha$-diimine$)_2$ (**2a–e**). Of these dimers, **2d,e** were thermally unstable at room temperature. They decomposed into their radicals, which were characterized with ESR in the case of **2d**. Complexes **1b–e** showed a side reaction at room temperature, giving rise to the formation of $(CO)_4Mn(\sigma$-*N*,σ-*N*′,η^2-*CN*-iPr-pyca$)Mn(CO)_3$ (**3b**) and $(CO)_3Mn(\sigma$-*N*,σ-*N*′,η^2-*CN*,η^2-*C*′*N*′-R-DAB) (**4c–e**), respectively. The crystal structure of **3b** was determined, and the data are as follows: monoclinic, $P2_1/a$, with a = 15.425 (1) Å, b = 9.867 (1) Å, c = 12.988 (1) Å, β = 111.310 (9)°, and Z = 4; R = 0.041. Both Mn atoms possess a distorted octahedral geometry, and the Mn–Mn distance is shorter than that in $Mn_2(CO)_{10}$. The formation of these complexes **3b**, **4c–e** was quenched by radical scavengers and favored in viscous solvents such as paraffin. At lower temperatures, the quantum yields for the photoproduction of **2–4** decreased, and in the case of **1c**, a novel complex, **5c**, was formed at $T \cong 180$ K by reaction of the $Mn(CO)_3$(iPr-DAB) radicals. **5c** was identified as $Mn_2(CO)_4(\sigma$-*N*,σ-*N*′,η^2-*CN*-iPr-DAB$)_2$. Raising the temperature above 180 K caused a thermal conversion of **5c** into $Mn_2(CO)_5(\sigma$-*N*,σ-*N*′-iPr-DAB$)(\sigma$-*N*,σ-*N*′,η^2-*CN*-iPr-DAB) (**6c**). A further increase of temperature above 200 K caused the formation of **2c** out of **6c**. At temperatures below 183 K, homolysis products were no longer formed, but instead the CO-loss complexes $(CO)_4Mn(\mu$-CO$)Mn(CO)_2(\alpha$-diimine) (**7**) were produced. The thermal and photochemical reactions of the CO-bridged complex **7a** were studied. For both primary photoprocesses, homolysis and release of CO, the quantum yields were high and wavelength independent throughout the MLCT band. They are therefore proposed to occur from the same $^3\sigma_b\sigma^*$ state of the complex after intersystem crossing/internal conversion from the MLCT state(s). The relative quantum yields of homolysis and CO-loss reactions resemble the ones that were derived for $Mn_2(CO)_{10}$, which points to a similar mechanism for the photochemistry of both types of complexes.

Introduction

In recent years, the mechanistic aspects of the photoreactions of the metal–metal-bonded carbonyls $M_2(CO)_{10}$ (M = Mn, Re), $Cp_2Fe_2(CO)_4$ and $Cp_2M_2(CO)_6$ (M = Mo, W) have received considerable attention.[1-3] Irradiation of these complexes gives rise to homolytic splitting of the metal–metal bond and release of CO as primary photoprocesses. The homolysis reaction occurs from the repulsive $^3\sigma_b\sigma^*$ state of the metal–metal bond; the CO-loss reaction has been proposed to take place from a LF state.[2] Substitution of two carbonyl groups by an α-diimine ligand produces highly colored complexes with low-lying metal to α-diimine charge-transfer (MLCT) transitions. The spectroscopy, photophysics, and photochemistry of several of these derivatives, viz. $L'_mM'M(CO)_3(\alpha$-diimine) (L'_mM' = $(CO)_5M'$ (M′ = Mn, Re),[4] $(CO)_4Co$,[5] $Cp(CO)_2Fe$,[6] Ph_3Sn;[7] M = Mn, Re) have been studied in detail and reviewed recently.[3,8] Irradiation into the MLCT band of these complexes (λ_{max} = 500–600 nm) gives rise to an efficient photoreaction with quantum yields varying between 0.3 and 0.9 mol/einstein. Although this reaction normally involves homolysis of the metal–metal bond, release of CO appeared to be the major reaction for $Ph_3SnMn(CO)_3(\alpha$-diimine)[7c] and the only one for $(CO)_5ReMn(CO)_3(\alpha$-diimine).[9] In the case of $(CO)_5MnMn(CO)_3(\alpha$-diimine), irradiation at room temperature gave only rise to the formation of homolysis products,[4a,b] although a recent nanosecond-flash photolysis study of $(CO)_5MnMn(CO)_3$(phen) has shown that both homolysis and release of CO are primary photoprocesses for this complex too.[10] The experimental data obtained so far for the abovementioned $L'_mM'M(CO)_3(\alpha$-diimine) complexes suggest that the homolysis and CO-loss reactions occur from the same repulsive $^3\sigma_b\sigma^*$ state after intersystem crossing/internal conversion from the MLCT state(s). Their quantum yields depend on the relative strengths of the M–M′ and M–CO bonds in this reactive state.

An interesting property of the $Mn(CO)_3(\alpha$-diimine) radicals formed by the reaction of the $(CO)_5MnMn(CO)_3(\alpha$-diimine) complexes is their ability to initiate electron-transfer chain reactions in the presence of a stabilizing nucleophile.[11] Thus, when a small amount of such a complex is added to a room temperature solution of $Ru_3(CO)_{12}$ and PPh_3, $Ru_3(CO)_{11}(PPh_3)$ is formed instantaneously as long as light is not completely excluded, whereas no such reaction is observed in the absence of the $(CO)_5MnMn(CO)_3(\alpha$-diimine) complex.

However, the $Mn(CO)_3(\alpha$-diimine) radicals cannot only give rise to electron-transfer reactions. In this article, we present evidence that they can also undergo radical coupling reactions for the case where the α-diimine ligand possesses one (R-pyca) or two (R-DAB) reactive CN bonds.

* To whom correspondence should be addressed.
† Part 7: Reference 5.
‡ Anorganisch Chemisch Laboratorium.
§ Laboratorium voor Kristallografie.
‖ Present address: AKZO Research Laboratories Arnhem, P.O. Box 9300, 6800 SB Arnhem, The Netherlands.

(1) Geoffroy, G. L.; Wrighton, M. S. *Organometallic Photochemistry*; Academic Press: New York, 1979.
(2) Meyer, T. J.; Caspar, J. V. *Chem. Rev.* **1985**, *85*, 187.
(3) Stufkens, D. J. Steric and Electronic Effects on the Photochemical Reactions of Metal-Metal Bonded Carbonyls. In *Stereochemistry of Organometallic and Inorganic Compounds*; Bernal, I., Ed.; Elsevier: Amsterdam, 1989; Vol. 3, p 226.
(4) (a) Morse, D. L.; Wrighton, M. S. *J. Am. Chem. Soc.* **1976**, *98*, 3931. (b) Kokkes, M. W.; Stufkens, D. J.; Oskam, A. *Inorg. Chem.* **1985**, *24*, 2934. (c) Kokkes, M. W.; de Lange, W. G. J.; Stufkens, D. J.; Oskam, A. *J. Organomet. Chem.* **1985**, *294*, 59. (d) Kokkes, M. W.; Stufkens, D. J.; Oskam, A. *Inorg. Chem.* **1985**, *24*, 4411.
(5) van Dijk, H. K.; van der Haar, J.; Stufkens, D. J.; Oskam, A. *Inorg. Chem.* **1989**, *28*, 75.
(6) Servaas, P. C.; Stor, G.; Stufkens, D. J.; Oskam, A. *Inorg. Chim. Acta*, in press.
(7) (a) Luong, J. C.; Faltynek, R. A.; Wrighton, M. S. *J. Am. Chem. Soc.* **1979**, *101*, 1597. (b) Luong, J. C.; Faltynek, R. A.; Wrighton, M. S. *J. Am. Chem. Soc.* **1980**, *102*, 7892. (c) Andrëa, R. R.; Stufkens, D. J.; Oskam, A. *Inorg. Chem.* **1989**, *28*, 318.
(8) Stufkens, D. J. *Coord. Chem. Rev.* **1990**, *104*, 39.
(9) van der Graaf, T.; van Rooij, A.; Stufkens, D. J.; Oskam, A. To be published.
(10) Yasufuku, K.; Sakamoto, H. Personal Communication.
(11) van der Graaf, T.; Hofstra, R.; Schilder, P. G. M.; Rijkhoff, M.; Stufkens, D. J.; Oskam, A.; van der Linden, W. G. J. To be published.

0020-1669/91/1330-0599$02.50/0

Table I. CO Stretching Frequencies and MLCT Band Positions for **1a–e** in Toluene at 298 K

complex	α-diimine	ν(CO), cm^{-1}						λ_{max}^{MLCT}, nm
1a	bpy′	2055 m		1982 s	1953 s		1901 m	550
1b	iPr-pyca	2057		1981	1961		1903	582
1c	iPr-DAB	2064	1997 w	1983	1973		1909	557
1d	pTol-DAB	2070		1992	1984	1957 w	1913	606
1e	pAn-DAB	2076	2004	1970		1962	1909	590

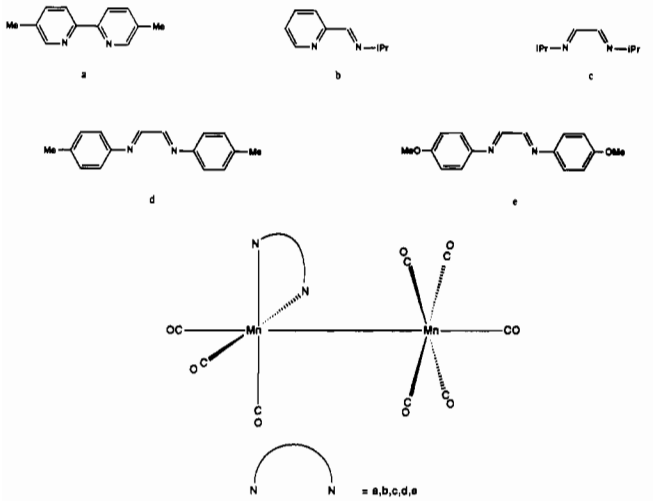

Figure 1. α-Diimine ligands a–e and the general molecular structure of **1**.

It will also be shown that, although irradiation of these $(CO)_5MnMn(CO)_3$(α-diimine) complexes only leads to the formation of homolysis products at $T > 183$ K, release of CO is the sole reaction taking place at temperatures just above the melting point of the solvent where it becomes very viscous.

The α-diimine ligands used in the course of this study are as follows: 4,4′-dimethyl-2,2′-bipyridine (bpy′, a), pyridine-2-carbaldehyde N-isopropylimine (iPr-pyca, b), 1,4-diisopropyl-1,4-diaza-1,3-butadiene (iPr-DAB, c), 1,4-di-*p*-tolyl-1,4-diaza-1,3-butadiene (pTol-DAB, d), 1,4-di-*p*-anisyl-1,4-diaza-1,3-butadiene (pAn-DAB, e). The structures of these molecules (a–e) and of their $(CO)_5MnMn(CO)_3$(α-diimine) complexes (**1a–e**) are schematically depicted in Figure 1.

Experimental Section

Materials and Preparations. THF, 2-MeTHF, and toluene were dried and distilled under a nitrogen atmosphere in the presence of sodium, alkanes in the presence of P_2O_5, and CCl_4 and CH_2Cl_2 in the presence of $CaCl_2$. Paraffin (Merck, Uvasol) was used without further purification. All solvents were stored in Schlenk flasks and carefully handled to exclude water and oxygen. $P(nBu)_3$ and $P(OMe)_3$ were distilled under vacuum over CaH_2 and stored under nitrogen. PPh_3 was recrystallized from a *n*-hexane solution. Bpy′ (a) (Merck) was used without further purification, iPr-pyca (b), iPr-DAB (c), pTol-DAB (d) and pAn-DAB (e) were synthesized by literature procedures.[12] The complexes $(CO)_5MnMn(CO)_3$(α-diimine) (**1a–e**) were prepared as previously described.[4a,13]

The photoproducts $(CO)_4Mn(\sigma\text{-}N,\sigma\text{-}N',\eta^2\text{-}CN$-iPr-pyca)$Mn(CO)_3$ (**3b**), $(CO)_3Mn(\sigma\text{-}N,\sigma\text{-}N',\eta^2\text{-}CN$, $\eta^2\text{-}C'N'$-iPr-DAB)$Mn(CO)_3$ (**4c**), and $(CO)_3Mn(\sigma\text{-}N,\sigma\text{-}N',\eta^2\text{-}CN,\eta^2\text{-}C'N'$-pTol-DAB) (**4d**) were made on a preparative scale by irradiation of 1 mmol of **1b**, **1c**, and **1d**, respectively, in 50 mL of THF with 546-nm light. The reaction was followed with IR spectroscopy, and the irradiation was stopped when **1** had completely disappeared. The solvent was evaporated, and the product was eluted with *n*-hexane on a silica column. The red fraction was collected and recrystallized from n-hexane.

Table I presents the IR ν(CO) frequencies and maxima of the MLCT bands for complexes **1a–e**; the molecular weights, IR, ^{1}H NMR, and UV/vis data of the photoproducts **3b**, **4c**, and **4d** are collected in Table VI.

Spectroscopic Measurements. IR spectra were recorded on a Nicolet 7199 B FTIR spectrophotometer by using a liquid-nitrogen-cooled MCT detector (32 scans, resolution 1.0 cm^{-1}).

Electronic absorption spectra were measured on a Perkin-Elmer Lambda 5 UV/vis spectrophotometer connected to a Model 3600 data station.

Low-temperature UV/vis and IR measurements were performed by using an Oxford Instruments DN 1704/54 liquid-nitrogen cryostat.

^{1}H NMR spectra were recorded on a Bruker AC 100 spectrometer; ESR spectra were recorded on a Bruker ER-200-D-MR X band spectrometer with 100-kHz modulation and temperature accessory. Coupling constants were obtained by computer simulation.

Photochemistry. For the photochemical reactions the complexes were irradiated by one of the lines of a Spectra Physics 2025 argon ion laser or a Model CR 490 tunable dye laser with Rhodamine 6G as a dye or by a Philips HPK 125 W high-pressure mercury lamp provided with the appropriate interference filter.

The samples for the quantum yield determinations were prepared in a room that was illuminated with red light. The cell containing the sample solution was then placed in a black box equipped with shutters on three sides. The solution was kept in this holder during transportation and irradiation. The box was constructed in such a way that irradiation could take place inside the UV/vis spectrophotometer via a glass fiber equipped with a mechanical shutter. This procedure prevented stray light from influencing the measurements. Quantum yields were all measured in duplicate. The setup was tested with ferrioxalate actinometry and with quantum yield data from the literature.

Crystal Structure Determination of 3b. The experimental details of the crystal structure determination of compound **3b** are listed in Table II.

Table II. Crystallographic Data for **3b**

chem formula	$C_{16}H_{12}N_2O_7Mn_2$
fw	454.18
space group	$P2_1/a$
a, Å	15.425 (1)
b, Å	9.867 (1)
c, Å	12.988 (1)
β, deg	111.310 (9)
V, Å^3	1841.6 (3)
Z	4
d_{calc}, g cm^{-3}	1.64
λ(Mo Kα), Å	0.71069
μ(Mo Kα), cm^{-1}	13.55
F(0,0,0)	912
T, K	293
R	0.041
R_w	0.073

A red monoclinic crystal with the dimensions 0.25 × 0.38 × 0.40 mm was used for data collection on an Enraf-Nonius CAD-4 diffractometer with graphite-monochromated Mo Kα radiation and a θ–2θ scan. A total of 8030 unique reflections were measured within the range $24 \le h \le 22$, $0 \le k \le 15$, $0 \le l \le 20$. Of these, 4160 were above the significance level of $2.5\sigma(I)$. The maximum value of $(\sin\theta)/\lambda$ was 0.80 Å^{-1}. Unit cell parameters were refined by a least-squares fitting procedure using 23 reflections with $46° < 2\theta < 50°$. Corrections for Lorentz and polarization effects were applied. The positions of the Mn atoms were determined by direct methods with the program SIMPEL.[14] From a ΔF synthesis, the rest of the non-hydrogen atoms were derived. After isotropic refinement the H atoms were derived from a subsequent ΔF synthesis. Block-diagonal least-squares refinement on F, anisotropic for the non-hydrogen atoms and isotropic for the hydrogen atoms, converged to $R = 0.041$, $R_w = 0.073$, and $(\Delta/\sigma)_{max} = 0.60$. A weighting scheme $w = (6.32 + F_o + 0.012(F_{obs})^2)^{-1}$ was used. An empirical absorption correction (DIFABS[15]) was applied with coefficients in the range of 0.69–1.14. A final difference Fourier map revealed a residual electron density be-

(12) Bock, H.; tom Dieck, H. *Chem. Ber.* **1967**, *100*, 228.
(13) Staal, L. H.; van Koten, G.; Vrieze, K. *J. Organomet. Chem.* **1979**, *175*, 73.
(14) Schenk, H.; Kiers, C. T. Simpel 83, a program system for direct methods. In *Crystallographic Computing*; Sheldrick, G. M., Ed.; Clarendon Press: Oxford, England, 1983.
(15) Walker, N.; Stuart, D. *Acta Crystallogr., Sect. A: Found. Crystallogr.* **1983**, *A39*, 158.

Table III. Fractional Coordinates with Estimated Standard Deviations (Esd's) in Parentheses

atom	x	y	z
Mn(1)	0.29498 (4)	0.39201 (5)	0.87828 (4)
Mn(2)	0.21097 (4)	0.52743 (5)	0.68114 (4)
C(1)	0.2959 (3)	0.5827 (4)	0.8791 (3)
C(2)	0.3144 (3)	0.4166 (4)	1.0249 (3)
C(3)	0.3220 (3)	0.2112 (4)	0.9094 (3)
C(4)	0.4128 (3)	0.4023 (5)	0.8773 (4)
C(5)	0.3078 (3)	0.4850 (4)	0.6394 (3)
C(6)	0.2348 (3)	0.7038 (4)	0.6654 (3)
C(7)	0.1324 (3)	0.5247 (5)	0.5392 (3)
C(8)	0.1499 (2)	0.3570 (4)	0.8137 (3)
C(9)	0.0918 (2)	0.4768 (4)	0.8024 (3)
C(10)	0.0230 (3)	0.4881 (5)	0.8487 (3)
C(11)	−0.0289 (3)	0.6048 (6)	0.8302 (4)
C(12)	−0.0113 (3)	0.7079 (5)	0.7690 (4)
C(13)	0.0566 (3)	0.6908 (4)	0.7244 (4)
N(1)	0.1921 (2)	0.3455 (3)	0.7347 (2)
N(2)	0.1077 (2)	0.5761 (3)	0.7402 (3)
O(1)	0.3120 (3)	0.6911 (3)	0.9099 (3)
O(2)	0.3269 (3)	0.4345 (4)	1.1153 (3)
O(3)	0.3442 (3)	0.1016 (4)	0.9323 (3)
O(4)	0.4875 (2)	0.4061 (5)	0.8804 (4)
O(5)	0.3685 (3)	0.4663 (4)	0.6105 (3)
O(6)	0.2497 (3)	0.8159 (4)	0.6542 (4)
O(7)	0.0839 (2)	0.5264 (4)	0.4489 (3)

Table IV. Selected Bond Lengths (Å) and Bond Angles (deg) with Esd's in Parentheses[a]

Mn(1)–Mn(2)	2.758 (1)	C(1)–O(1)	1.137 (4)
Mn(1)–C(1)	1.882 (3)	C(2)–O(2)	1.132 (4)
Mn(1)–C(2)	1.833 (3)	C(3)–O(3)	1.141 (4)
Mn(1)–C(3)	1.843 (3)	C(4)–O(4)	1.139 (5)
Mn(1)–C(4)	1.825 (4)	C(5)–O(5)	1.143 (5)
Mn(1)–C(8)	2.113 (3)	C(6)–O(6)	1.150 (4)
Mn(1)–N(1)	2.014 (2)	C(7)–O(7)	1.139 (4)
Mn(2)–C(5)	1.813 (4)	C(8)–C(9)	1.458 (4)
Mn(2)–C(6)	1.805 (3)	C(8)–N(1)	1.405 (4)
Mn(2)–C(7)	1.801 (3)	C(9)–N(2)	1.348 (4)
Mn(2)–N(1)	1.984 (2)	C(13)–N(2)	1.352 (4)
Mn(2)–N(2)	2.060 (3)		
Mn(2)–Mn(1)–C(1)	61.4 (1)	Mn(1)–Mn(2)–C(5)	90.3 (2)
Mn(2)–Mn(1)–C(2)	138.1 (1)	Mn(1)–Mn(2)–C(6)	121.7 (1)
Mn(2)–Mn(1)–C(3)	131.7 (1)	Mn(1)–Mn(2)–C(7)	149.0 (1)
Mn(2)–Mn(1)–C(4)	95.7 (2)	Mn(1)–Mn(2)–N(1)	46.82 (8)
Mn(2)–Mn(1)–C(8)	68.8 (1)	Mn(1)–Mn(2)–N(2)	86.2 (1)
Mn(2)–Mn(1)–N(1)	45.94 (8)	C(5)–Mn(2)–C(6)	88.0 (2)
C(1)–Mn(1)–C(2)	82.2 (2)	C(5)–Mn(2)–C(7)	90.7 (2)
C(1)–Mn(1)–C(3)	165.0 (2)	C(5)–Mn(2)–N(1)	97.9 (2)
C(1)–Mn(1)–C(4)	86.5 (2)	C(5)–Mn(2)–N(2)	175.9 (2)
C(1)–Mn(1)–C(8)	99.8 (2)	C(6)–Mn(2)–C(7)	89.3 (2)
C(1)–Mn(1)–N(1)	103.6 (2)	C(6)–Mn(2)–N(1)	166.7 (1)
C(2)–Mn(1)–C(3)	87.8 (2)	C(6)–Mn(2)–N(2)	92.0 (2)
C(2)–Mn(1)–C(4)	102.3 (2)	C(7)–Mn(2)–N(1)	102.4 (2)
C(2)–Mn(1)–C(8)	100.6 (2)	C(7)–Mn(2)–N(2)	93.5 (2)
C(2)–Mn(1)–N(1)	140.2 (2)	N(1)–Mn(2)–N(2)	81.3 (1)
C(3)–Mn(1)–C(4)	84.8 (2)	Mn(1)–C(8)–N(1)	66.3 (3)
C(3)–Mn(1)–C(8)	92.9 (2)	Mn(1)–N(1)–Mn(2)	87.2 (1)
C(3)–Mn(1)–N(1)	91.2 (2)	Mn(1)–N(1)–C(8)	74.0 (2)
C(4)–Mn(1)–C(8)	156.9 (2)	Mn(2)–N(1)–C(8)	110.4 (2)
C(4)–Mn(1)–N(1)	117.2 (2)	Mn(2)–N(2)–C(9)	112.8 (2)
C(8)–Mn(1)–N(1)	39.7 (1)	Mn(2)–N(2)–C(13)	128.7 (2)

[a] Mn(2)–C(1) distance (no bond length) is 2.485 Å.

tween −0.5 and +0.5 e Å^{-3}. Scattering factors were taken from Cromer and Mann.[16] Anomalous dispersion for Mn was corrected for. All calculations were performed with XRAY 76,[17] unless stated otherwise. The final positional parameters and the equivalent isotropic thermal parameters for the non-hydrogen atoms are given in Table III. The selected bond distances and angles of **3b** are collected in Table IV.

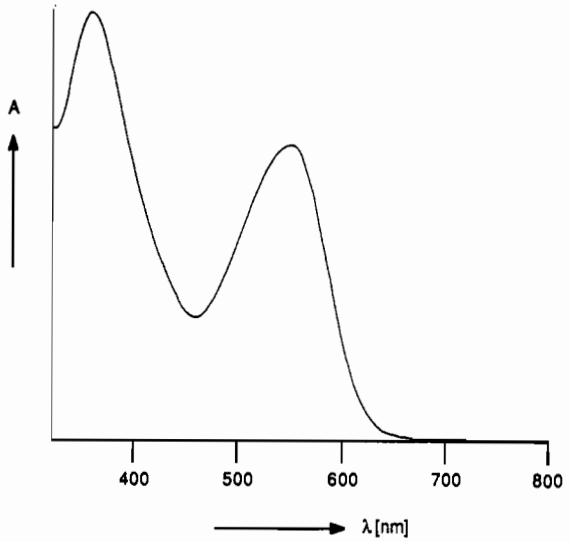

Figure 2. Electronic absorption spectrum of **1a** in toluene at room temperature.

Results and Discussion

Spectroscopic Properties. The IR spectra of **1a–e** (symmetry group C_s) display less than the eight expected carbonyl vibrations because of coincidence of bands (see Table I). However, all these bands have been detected before for other $(CO)_5MM'(CO)_3(\alpha$-diimine) (M, M′ = Mn, Re) complexes and assigned to the vibrations of the $M'(CO)_3(\alpha$-diimine) and the $M(CO)_5$ fragments.[18] A small influence of the α-diimine ligand on the carbonyl vibrations is best seen for the distinct band around 2060 cm^{-1} belonging to the a_1(eq) vibration of the $M(CO)_5$ (C_{4v}) group. Just as observed for the $\nu(CO)_{ax}$(a′) vibration of $Mn(CO)_3(\alpha$-diimine)X (X = Cl, Br) (C_s), this band shifts to higher wavenumbers in going from bpy′ to R-DAB, because of the better π-acceptor properties of the latter ligands.[19] One of the most conspicious features of **1a–e** is their intense absorptions in the visible region. A typical UV/vis absorption spectrum is presented in Figure 2. It shows two strong absorption bands, a sharp one around 350 nm and a broad band with a maximum between 500 and 600 nm.

The first band is assigned to the $\sigma_b \rightarrow \sigma^*$ transition of the Mn–Mn bond as it is close in energy to the corresponding transition of $Mn_2(CO)_{10}$ and shows the same characteristic sharpening and intensity increase at lower temperatures.[20] The second intense (ϵ = (5–12) × 10^3 M^{-1} cm^{-1}) band between 500 and 600 nm has been assigned before to $d_\pi(M) \rightarrow \pi^*(\alpha$-diimine) MLCT transitions for several $L'_mM'M(CO)_3(\alpha$-diimine) (M = Mn, Re) complexes.[5,8,18,21] This assignment was based on the solvatochromic behavior of these bands, characteristic for MLCT transitions, and on the results of the resonance Raman (rR) spectra. These spectra showed, just as those of the mononuclear complexes $M(CO)_4(\alpha$-diimine) (M = Cr, Mo, W), $M'(CO)_3(\alpha$-diimine) (M′ = Fe, Ru), and $Ni(CO)_2(\alpha$-diimine)[8] showed, resonance enhancement of Raman intensity for the α-diimine and metal–ligand stretching modes. From these rR effects it was concluded that the electronic transitions involved are MLCT in character. Furthermore, when one goes from the bpy and phen complexes to those of R-DAB the rR intensities of the metal–ligand vibrations appeared to increase at the expense of the ligand stretching modes. This means that the metal d_π and ligand π^* orbitals more strongly interact in the ground and lowest excited states in the case of the R-DAB

(16) Cromer, D. T.; Mann, J. B. *Acta Crystallogr., Sect. A: Cryst. Phys. Diffr. Theor. Gen. Crystallogr.* **1968**, *A24*, 321.
(17) Stewart, J. M.; Machin, P. A.; Dickinson, C. W.; Ammon, H. L.; Heck, H.; Flack, H. The XRay 76 system. Technical Report TR-446; Computer Science Center, University of Maryland: College Park, MD, 1976.
(18) Kokkes, M. W.; Snoeck, Th. L.; Stufkens, D. J.; Oskam, A.; Cristophersen, M.; Stam, C. H. *J. Mol. Struct.* **1985**, *131*, 11.
(19) tom Dieck, H.; Franz, K. D.; Hohmann, F. *Chem. Ber.* **1975**, *108*, 163. Andrêa, R. R.; de Lange, W. G. J.; van der Graaf, T.; Rijkhoff, M.; Stufkens, D. J.; Oskam, A. *Organometallics* **1988**, *7*, 1100.
(20) Wrighton, M. S.; Ginley, D. S. *J. Am. Chem. Soc.* **1975**, *97*, 2065.
(21) Andrêa, R. R.; de Lange, W. G. J.; Stufkens, D. J.; Oskam, A. *Inorg. Chim. Acta* **1988**, *149*, 77.

Table V. CO Stretching Frequencies and Absorption Maxima for **2a–e** in Toluene

complex	ν(CO), [cm^{-1}]				λ_{max}^{MLCT}, nm
2a[a]	1965 w	1938 s	1889 w	1863 m	805
2b[a]	1968	1943	1893	1887	818
2c[a]	1978	1950	1902	1887	754
2d[b]	1984	1958	1913	1898	840
2e[b]		1957	1910	1892	841

[a] 298 K. [b] 183 K.

Table VI. Quantum Yields of the Photoreaction of **1a** with CCl_4 in Toluene at Different Temperatures and Irradiation Wavelengths

λ_{irr},[a] nm	quantum yield (ϕ)					
	T = 298 K	T = 295 K	T = 285 K	T = 275 K	T = 265 K	T = 255 K
514	0.70					
555	0.70					
585	0.60	0.68	0.71	0.82	0.83	0.72
615	0.62					

[a] P_λ = 10 mW; ϕ in mol/einstein, estimated error 10%.

complexes. As a result, the MLCT character of the electronic transitions will decrease on going to the R-DAB complexes, and this conclusion was confirmed by the observation of a concomitant decrease of solvatochromism. The same rR behavior was observed for complexes **1a–e**.

Photochemical Reactions. The photochemical reactions of complexes **1a–e** were studied in different media at temperatures ranging from 133 K to room temperature. The reactions were followed by IR and UV/vis spectroscopy, and the spectroscopic data of the products formed are presented in Tables V, VII, X, XI, and XII.

Reactions at Room Temperature. Irradiation of a solution of **1a** in toluene into its MLCT band gave rise to an efficient photochemical reaction. The MLCT band disappeared, and a new band showed up at 850 nm, belonging to the dimeric species $Mn_2(CO)_6(bpy')_2$.[4c] This assignment was confirmed by the IR spectral data, which showed the formation of $Mn_2(CO)_{10}$ and the appearance of the characteristic CO-stretching modes of $Mn_2(CO)_6(bpy')_2$ at 1965, 1938, 1889, and 1863 cm^{-1} (Table V). These results, which agree with previous photochemical studies on these and related complexes,[8] show that the following reactions (eqs. 1–3) had occurred:

$$(CO)_5MnMn(CO)_3(bpy') \xrightarrow{h\nu} Mn(CO)_5 + Mn(CO)_3(bpy') \quad (1)$$

$$2Mn(CO)_5 \rightarrow Mn_2(CO)_{10} \quad (2)$$

$$2Mn(CO)_3(bpy') \rightarrow Mn_2(CO)_6(bpy')_2 \quad (3)$$

The homolytic splitting of the metal–metal bond (reaction 1) was also evident from the photochemical reaction of **1a** taking place in the presence of CCl_4 as a radical scavenger. $Mn(CO)_5Cl$ and $Mn(CO)_3(bpy')Cl$ were then formed as the only products.

The wavelength dependence of the quantum yield for this homolysis reaction was determined by irradiating a mixture of **1a** and CCl_4 in toluene at different wavelengths (514.5–615 nm) within the MLCT band. The quantum yields ϕ_{1a}, determined by following the decay of the MLCT band of **1a**, appeared to be high and wavelength independent ($\phi_{1a} \cong 0.66$ mol/einstein), all variations being within experimental error (see Table VI). Irradiation with 514.5-nm light at different temperatures did not show a regular temperature dependence for ϕ_{1a} between 255 and 300 K (Table VI), which means that the homolysis reaction has no energy barrier.

Whereas similar products were obtained for **1a–c**, a different reaction was observed for **1d** and **1e**. For these complexes, $Mn_2(CO)_{10}$ was still produced in a reasonable amount but only traces of **2d** were detected, while **2e** was not formed at all. This influence of the α-diimine ligand on the product formation will be discussed hereafter. Apart from this, the room-temperature

Scheme I

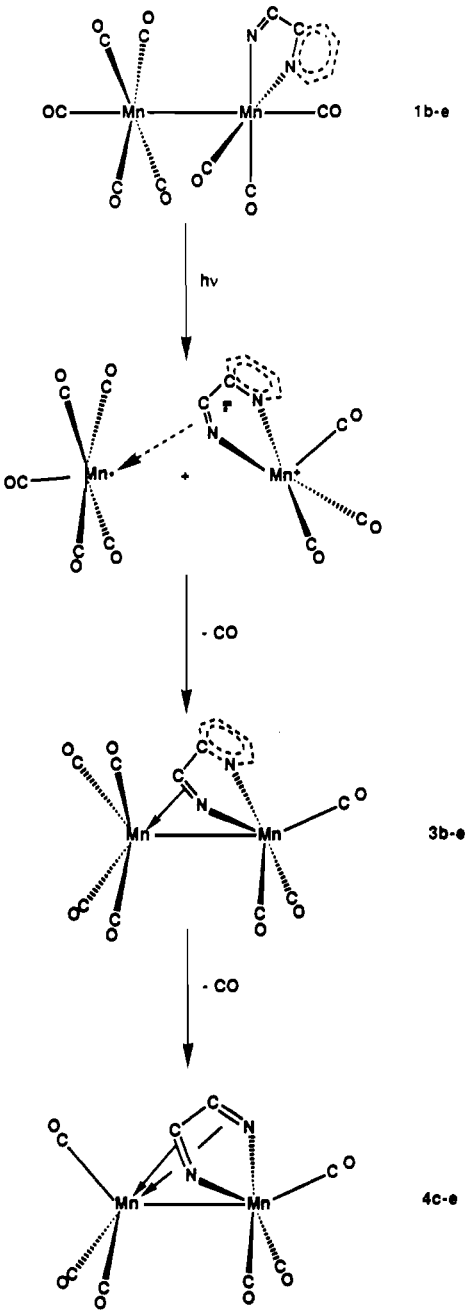

photochemistry of **1b–e** differed from that of **1a** by the formation of complexes **3b** and **4c–e**, respectively, which is shown schematically in Scheme I. In these photoproducts, the α-diimine bridges between two Mn fragments, a mode of coordination that cannot occur for the bpy' ligand of **1a**. Although the analogues of **3b**, **3c–e**, could not be detected, they are assumed to be reactive intermediates in the formation of **4c–e** out of **1c–e**.

The structure of **3b** has been established by an X-ray structure determination (vide infra); those of **4c–e** are similar to the ones of $(CO)_3Mn(\sigma\text{-}N,\sigma\text{-}N',\eta^2\text{-}CN,\eta^2\text{-}C'N'$-R-DAB)$Mn(CO)_3$ (vide infra), for which crystal structures have been determined.[22a,b] This similarity is evident from the close analogy between the ^{1}H NMR and IR spectra of these complexes (Table VII). A reaction similar to those observed for **1c–e** has been observed by us before for $(CO)_5MnRe(CO)_3$(iPr-DAB) in a CH_4 matrix and for the complexes $(CO)_5M'M(CO)_3$(iPr-DAB) (M, M' = Mn, Re except M, M' = Re) in a PVC film at 293 K.[4d]

(22) Motz, P. L.; Williams, J. P.; Alexander, J. J.; Ho, D. M.; Ricci, J. S.; Miller, W. T., Jr. *Organometallics* **1989**, *8*, 1523. Adams, R. D. *J. Am. Chem. Soc.* **1980**, *102*, 7476.

Table VII. FD Mass, IR, and ^{1}H NMR Data for **3b**, **4c–e**, and Related Compounds

complex	FD MS M_{obs} (M_{calc})	IR ν(CO),[a] cm^{-1}								^{1}H NMR δ, ppm (multiplicity, m H)[b]
3b	454 (454.18)	2049 m	2011 s	1995 s	1954 s	1941 m	1924 w	1909 w		7.89 (d, 1 H), 6.42 (m, 2 H), 5.75 (m, 1 H), 2.96 (s, 1 H), 2.65 (sept, 1 H), 1.47 (d, 3 H), 1.16 (d, 3 H)
3b[c]		2051	2006	1972	1944		1922	1912	1844 w	
4c	418 (418.20)	2030		1997	1949	1933	1920	1914		5.08 (s, 2 H), 2.40 (sept, 2 H), 0.99 (d, 6 H), 0.74 (d, 6 H)
4d	514 (514.28)	2037		1991	1949	1942		1917		6.68 (s, 8 H), 5.53 (s, 2 H), 1.92 (s, 6 H)
4e		2034		1995	1945	1935		1915		
4f[d]		2035		1998	1940	1935	1926	1917		3.02 (s, 6 H), 2.02 (s, 6 H)
4g[e]		2038		2006	1958			1916		7.24–6.41 (m, 16 H), 2.28 (s, 6 H), 3.74 (d, 4 H)

[a] In toluene. [b] Relative to Me_4Si; in C_6D_6; s = singlet, d = doublet, sept = septet, and m = multiplet. [c] In KBr. [d] α-Diimine = Me-DAB(Me,-Me).[22b] [e] α-Diimine = pTol-DAB(pCl–Ph–CH_2–, pCl–Ph–CH_2–).[22a]

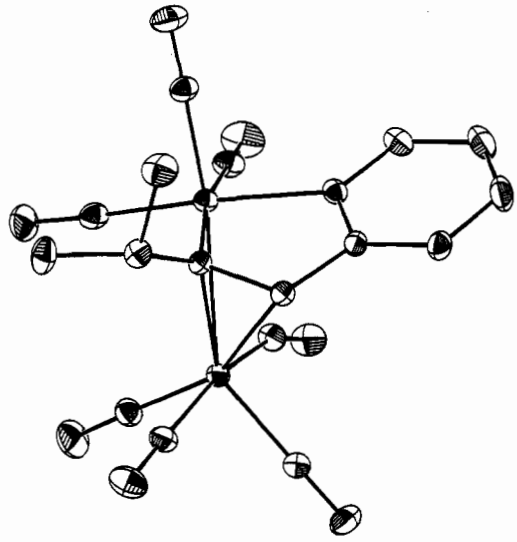

Figure 3. Crystal structure of **3b** (ORTEP drawing).

Molecular Structure of 3b. An ORTEP drawing of **3b** is presented in Figure 3. Both Mn atoms possess a distorted octahedral geometry. The Mn(1)Mn(2) bond distance of 2.758 Å is in-between those of $Mn_2(CO)_{10}$ (2.9038 Å)[23] and $(CO)_3Mn(\sigma\text{-}N,\sigma\text{-}N',\eta^2\text{-}CN,\eta^2\text{-}C'N'$-R-DAB)$Mn(CO)_3$ (2.613 Å for Ph-DAB(Ph,Ph),[22a] 2.615 Å for Me-DAB(Me,Me),[22b] 2.633 Å for pTol-DAB(pCl–Ph–CH_2–,pCl–Ph–CH_2–)[22a]). The iPr-pyca ligand is σ-N(1),σ-N(2)-bonded to Mn(2) and η^2-C(8)N(1) coordinated to Mn(1).

The N(2)C(9)C(8)N(1) α-diimine skeleton is not planar as in the σ,σ-bonded ligand. As a result of the η^2-coordination, the C(8)N(1) bond is twisted by 18° around the C(8)C(9) axis. The pyridine group has a planar structure with a C(9)N(2) distance of 1.348 Å, which is usual for the C=N group in a σ-N,σ-N′-bonded 2,2′-bipyridine ligand.[24a,b] This means that the pyridine ring is not influenced by the η^2-coordination. Because of its 4-electron bonding mode, the C(8)N(1) bond (1.405 Å) is elongated compared to the C=N bond distance of 1.258 Å in cHex-DAB[25] and of 1.301 Å for the σ,σ-bonded iPr-DAB ligand in $(CO)_5ReMn(CO)_3$(iPr-DAB).[18] The value is close to the 1.390-Å bond lengths of the corresponding C=N groups of $(CO)_3Mn(\sigma\text{-}N,\sigma\text{-}N',\eta^2\text{-}CN,\eta^2\text{-}C'N'$-Me-DAB(Me,Me))$Mn(CO)_3$.[22b] Six CO groups are bonded in a terminal fashion. C(1)O(1) is bent by 20° and its semibridging mode is reflected in its asymmetry parameter α = 0.3, which is within the range $0.1 < \alpha < 0.6$ for semibridging CO ligands.[26] The lowest CO-stretching frequency in the solid and solution is 1844 and 1912 cm^{-1}, respectively (see Table VII), which means that this ligand only forms a semibridge in the solid.

Table VIII. Normalized Yield of **4c**, x[**4c**], as a Function of the Molar Ratios $n[CCl_4]/n$[**1c**] (A) and $n[Mn_2(CO)_{10}]/n$[**1c**] (B) and Irradiation Wavelength λ_{irr} (C) in Hexane at 298 K

A		B		C	
$n[CCl_4]/n$[**1c**]	x[**4c**][a]	$n[Mn_2(CO)_{10}]/n$[**1c**]	x[**4c**][a]	λ_{irr}, nm	x[**4c**]
0	1.0	0	1.0	351/364[b]	4.6
5	0.9	1	1.2	488	1.5
75	0.3	13	1.3	540	1.3
400	0.0			570	1.1
				600	1.0

[a] λ_{irr} = 405 nm. [b] Unresolved UV lines of argon ion laser; increased value of x[**4c**] because of concomitant $Mn_2(CO)_{10}$ photoreaction.

The mechanism of the formation of **3b** and **4c–e** was established by studying the photoproduction of **4c** out of **1c** under various conditions. First of all, different amounts of CCl_4 (Table VIIIA) or $Mn_2(CO)_{10}$ (Table VIIIB) were added to a sample taken from a stock solution of **1c** in n-hexane. The solutions were then irradiated with 405-nm light, and the reactions were followed by IR spectroscopy. When **1c** had completely reacted away, the yield of **4c** was determined from the intensity of its carbonyl band at 1941 cm^{-1}, $I_{f,1941}$(**4c**). These values of $I_{f,1941}$(**4c**) were all normalized to $I^0_{f,1941}$(**4c**), the intensity of the 1941-cm^{-1} band when the reaction was performed in the absence of a substrate. These normalized values are denoted as x[**4c**] in Table VIIIA,B. The same procedure was followed for the study of the wavelength dependence of x[**4c**]. In that case, however, the value of $I_{f,1941}$(**4c**) were normalized to $I^0_{f,1941}$(**4c**) measured upon irradiation with 600 nm (Table VIIIC).

Addition of a small amount of CCl_4 to a solution of **1c** completely quenched the formation of $Mn_2(CO)_{10}$ and **2c**. A different behavior was, however, observed for **4c**, since the concentration of this photoproduct gradually decreased with increasing concentration of CCl_4. The formation of **4c** was only completely prevented when a large excess of CCl_4 was added to the solution (see Table VIIIA).

In order to study the influence of added CO, samples were taken from a 3.2×10^{-6} M solution of **1c** in n-hexane before and after saturation with CO. Saturation was achieved by bubbling a stream of CO through a solution that was already under a CO atmosphere. In this way a solution with a CO/**1c** concentration ratio of 4.1 was obtained, taking into account the earlier reported solubility coefficient for CO in n-hexane at 293 K, α = 0.014 mol dm^{-3} bar^{-1}.[27] Irradiation of these two solutions did not give rise to any difference in product formation.

Although the yield of **4c** did not change for $\lambda_{irr} > 514.5$ nm, it appeared to increase when the wavelength of irradiation was

(23) Churchill, M. R.; Amoh, K. N.; Wasserman, H. J. *Inorg. Chem.* **1981**, *20*, 1609.
(24) van Dijk, H. K.; Stufkens, D. J.; Oskam, A.; Rotteveel, M.; Heijdenrijk, D. *Organometallics* **1987**, *6*, 1665. Bruce, M. I.; Humphrey, M. G.; Snow, M. R.; Tiekink, E. R. T.; Wallis, R. C. *J. Organomet. Chem.* **1986**, *314*, 311.
(25) Keijsper, J.; van der Poel, H.; Polm, L.; van Koten, G.; Vrieze, K.; Seignette, P.; Varenhorst, R.; Stam, C. *Polyhedron* **1983**, *2*, 1111.
(26) Curtis, M. D.; Han, K. R.; Butler, W. M. *Inorg. Chem.* **1980**, *19*, 2096.
(27) Bor, G.; Dietler, U. K.; Pino, P.; Poë, A. *J. Organomet. Chem.* **1978**, *154*, 301.

Table IX. Product Ratio $n[Mn_2(CO)_{10}]/n[4c]$ after Photolysis of **1c** in Different Media

solvent	T, K	$n[Mn_2(CO)_{10}]/n[4c]^a$
paraffin	256	2.2
paraffin	298	5.7
n-hexane	256	8.2

$^a\lambda_{irr}$ = 586 nm, P_λ = 15 mW; $I_{f,2012}(Mn_2(CO)_{10})/I_{f,1941}(4c)$.

varied from 514.5 to 351 nm (Table VIIIB). The reason for this wavelength dependence became clear when $Mn_2(CO)_{10}$ was added to a solution of **1c** before irradiation. The yield of **4c** then increased for $\lambda_{irr} < 514.5$ nm, but this was not the case when a longer wavelength of irradiation was used (Table VIIIC). Apparently, the yield of **4c** depends on the concentration of $Mn(CO)_5$ radicals present in the solution. After irradiation of **1c**, these radicals will dimerize to give $Mn_2(CO)_{10}$ unless a wavelength of irradiation is used at which this dimer photodecomposes again into $Mn(CO)_5$ radicals. This will be the case for $\lambda_{irr} < 514.5$ nm, since $Mn_2(CO)_{10}$ does not absorb at longer wavelengths. The same wavelength dependence was observed for reaction 4 between $Mn_2(CO)_{10}$ and CCl_4, which only proceeds at $\lambda_{irr} < 514.5$ nm.

$$Mn_2(CO)_{10} + CCl_4 \xrightarrow{h\nu} 2Mn(CO)_5Cl \qquad (4)$$

Finally, the formation of **4c** was favored in viscous media, in which the lack of diffusion hampers the dimerization of the $Mn(CO)_5$ and $Mn(CO)_3$(iPr-DAB) radicals. When a solution of **1c** in paraffin at 256 K, just above its freezing point, was irradiated with λ = 514.5 nm, the concentration ratio of $Mn_2(CO)_{10}$ and **4c** was only 2.2, whereas a ratio of 8.2 was obtained in *n*-hexane at room temperature (Table IX). In completely rigid media such as solid paraffin at 173 K or a PVC film at room temperature, complex **4c** was the only product formed. The above results show that a competition exists between the formation of $Mn_2(CO)_{10}$ and **2c** on one side and of **4c** on the other. Besides, they give conclusive evidence for the mechanism of formation of **4c**, which will be discussed further in a later Section.

Addition of extra $Mn_2(CO)_{10}$ to a solution of **1c** only increased the photoproduction of **4c** when $\lambda_{irr} \leq 514.5$ nm. Apparently, **4c** cannot be formed by reaction of $Mn(CO)_3$(iPr-DAB) radicals with $Mn_2(CO)_{10}$ but only with $Mn(CO)_5$ radicals (Scheme I). This conclusion was confirmed by the thermal reaction between $Mn_2(CO)_{10}$ and $Mn_2(CO)_6$(iPr-DAB)$_2$ (**2c**), both formed photochemically out of **1c**. This reaction was allowed to proceed in the dark after completion of the photoreaction. After 24 h, no extra **4c** was then formed, although the dimers **2** are known to be partly split into their radicals according to reaction 3.[19b] However, although $Mn_2(CO)_{10}$ and **2c** did not produce **4c**, they appeared to react back slowly with each other to give the parent compound **1c**. Apparently, attack of the $Mn(CO)_3$(iPr-DAB) radicals on $Mn_2(CO)_{10}$ gives rise to the formation of a different product, viz. **1c**, than when they react with $Mn(CO)_5$ radicals (**4c**). The yield of **1** out of $Mn_2(CO)_{10}$ and **2** strongly depended on the α-diimine ligand. After 24 h, $Mn_2(CO)_{10}$ and **2a** had reacted back by 60% to give **1a**, whereas this percentage was 30% for **1b** and only 10% for **1c**.

Reactions at 183 K < T < 298 K. In contrast to those of **1b–e**, the reaction of **1a** did not depend on the temperature. Photolysis of **1b** gave rise to the formation of a very complicated CO band pattern in the IR, which could not further be analyzed. Finally, the reactions taking place for **1c** and **1d,e**, respectively, differed from each other, and they will therefore be discussed hereafter separately.

Reaction of 1c. Lowering the temperature gave rise to a regular decrease of the quantum yield for the photoproduction of **2c** and **4c**, and below 200 K, two new complexes, **5** and **6**, were formed. Due to their thermal instability, these products could neither be isolated nor be characterized by ^{1}H NMR. Information about their structures and the mechanism of their formation and thermal decomposition (Scheme II), was therefore derived mainly from the IR and UV/vis spectra. Both complexes are reactive intermediates, **5c** being only stable at temperatures below 180 K.

Scheme II

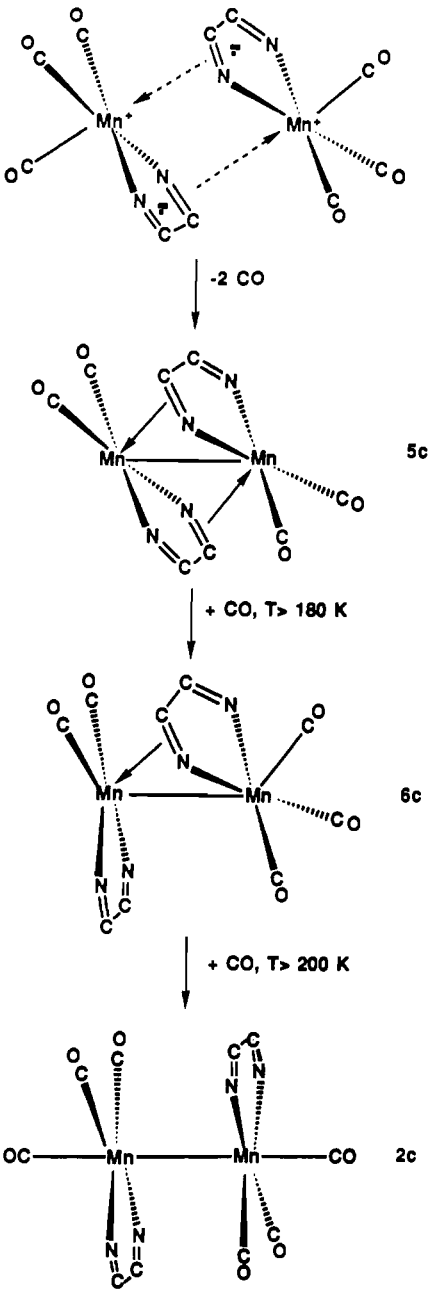

Above this temperature it converted thermally into **6c**, which in turn produced **2c** when the temperature was raised above 200 K. During these latter reactions, the concentration of $Mn_2(CO)_{10}$ did not change, which means that **5c** and **6c** are the only precursors for the formation of **2c** and most probably contain two $Mn(CO)_x(\alpha$-diimine) fragments just as the latter complex. Both **5c** and **6c** were formed in toluene and CH_2Cl_2 as well as 2-MeTHF with almost the same CO-stretching frequencies and electronic absorption spectra. This means that these complexes are coordinatively saturated species and do not contain a solvent molecule.

The formation of **5c** was accompanied by the disappearance of the MLCT band. This may be due to either breakage of a metal–nitrogen bond or to η^2-coordination of one or both CN bonds of the iPr-DAB ligand. The latter possibility is much more likely since the corresponding bpy′ complex **5a** was not formed by photolysis of **1a**.

The thermal conversion of **5c** into **6c** was accompanied by the reappearance of a MLCT band close in energy to that of **2c**. Apparently, **5c** contains two η^2-CN bonds from which one is broken upon thermal conversion into **6c**. The open site thus obtained will be occupied by CO still present in the solution. The influence of CO on this conversion of **5c** into **6c** was demonstrated

Table X. CO Stretching Frequencies and Absorption Maxima of **5c**, **6c**, and Related Compounds

complex	ν(CO), cm^{-1}					λ_{max}^{MLCT}, nm
5c[a]				1969 s	1896 m, br	···
5c[b]				1967	1892	···
6c[a]	2101 w	2024 m	1994 m	1948 s	1864 m	795
6c[c]	2101	2026	1992	1945	1860	790
$Ru_2(CO)_4(\sigma\text{-}N,\sigma\text{-}N',\eta^2\text{-CN-}\alpha\text{-diimine})$						
α-diimine = cHex-DAB[d]				1974 s	1905 m	
α-diimine = iPr-DAB[d]				1983	1922	
α-diimine = iPr-pyca[e]				1971	1904	

[a] In 2-MeTHF; 173 K. [b] In CH_2Cl_2; 183 K. [c] In toluene; 183 K. [d] Reference 28a. [e] Reference 18b.

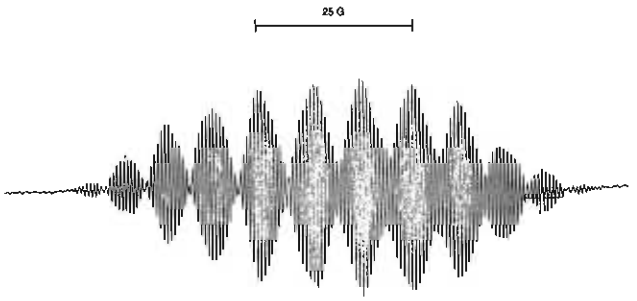

Figure 4. ESR spectrum of $Mn(CO)_3$(pTol-DAB) in toluene at 253 K.

by saturating a 2-MeTHF solution of **1c** with CO before irradiation. Photolysis at 173 K then gave rise to the formation of **6c** as the only product. On the basis of these results structures are proposed for **5c** and **6c** that are depicted in Scheme II. From these, the structure of **5c** could be confirmed by comparison of its CO-stretching frequencies with those of the stable complexes $Ru_2(CO)_4(\sigma\text{-}N,\sigma\text{-}N',\eta^2\text{-}CN\text{-R-DAB})_2$ and $Ru_2(CO)_4(\sigma\text{-}N,\sigma\text{-}N',\eta^2\text{-}CN\text{-R-pyca})_2$, for which both IR and crystal structure data are available.[28] In both cases the IR spectra (Table X) show the presence of only two CO-stretching modes in agreement with a trans conformation for these complexes. The Ru and Mn complexes will have a similar structure apart from the metal–metal bond, which will only be present in the Mn complex **5c**, which has the formula $Mn_2(CO)_4(\sigma\text{-}N,\sigma\text{-}N',\eta^2\text{-}CN\text{-iPr-DAB})_2$. To our knowledge no analogue of **6c** has been reported so far in the literature. However, all data are in favor of the structure presented in Scheme II and so are the five IR CO-stretching frequencies, which point to the presence of at least five terminal carbonyls in this complex. The complex has the formula $Mn_2(CO)_5(\sigma\text{-}N,\sigma\text{-}N'\text{-iPr-DAB})(\sigma\text{-}N,\sigma\text{-}N'\text{-}\eta^2\text{-}CN\text{-iPr-DAB})$. The mechanism of the reaction sequence of Scheme II will be discussed hereafter.

Reactions of 1d,e. As mentioned before, irradiation of **1d,e** produced $Mn_2(CO)_{10}$ and **4d,e** but only very small amounts of **2d,e**. The yield of **2d,e** increased however when the photoreaction was performed at lower temperatures. At 183 K, a complete conversion of **1d,e** into $Mn_2(CO)_{10}$ and **2d,e** was observed. Raising the temperature of the solution after photolysis gave rise to decomposition of **2d,e** into **1d,e** and unidentified tricarbonyl species. In the case of **2d**, this decomposition was followed by ESR spectroscopy. For this purpose, a solution of **1d** was irradiated at 183 K with 546-nm light in the microwave cavity of the ESR spectrometer. ESR signals only showed up when the temperature of the product solution was raised. Figure 4 presents the ESR spectrum recorded at 253 K; a further rise of temperature caused a regular decrease of intensity and finally the complete disappearance of the signal at 273 K.

The ESR spectrum consists of 12 groups of nicely ordered multiplets. It was simulated with one Mn nucleus ($I = {}^5/_2$, a_{Mn} = 7.84), two nitrogen atoms (I = 1, a_N = 6.92), two protons ($I = {}^1/_2$, a_H = 6.0), and a hyperfine splitting of four ortho and four meta protons of the pTol groups (a_{H_o} = 1.38, a_{H_m} = 0.46). The large coupling constants for the α-diimine nitrogen and imine protons were also observed in the ESR spectra of $Mn(CO)_3$(tBu-DAB),[19b] $Re(CO)_3(\alpha\text{-diimine})$,[19b] and $Cr(CO)_4(\alpha\text{-diimine})^-$[29] radicals. Together with the g value (g = 2.0018), they imply that the unpaired electron of these radicals is mainly localized at the α-diimine ligand. The nitrogen and aryl proton coupling constants of the radical observed here are very similar to those of $Cr(CO)_4$(Ph-DAB)$^-$ (a_N = 5.7, a_{H_o} = 1.35, a_{H_m} = 0.56, a_{H_p} = 1.94) and $Cr(CO)_4$(Ph-DAB(Me,Me))$^-$, (a_N = 5.67, a_{H_o} = 1.25, a_{H_m} = 0.69, a_{H_p} = 1.97).[29] For these latter radicals, it had been found that the coupling constants of the ortho and meta protons are insensitive toward substitution of the para group (a_N = 5.7, a_H = 3.72, a_{H_o} = 1.38, a_{H_m} = 0.66 for $Cr(CO)_4$(pAn-DAB)$^-$). The ESR spectrum in Figure 4 thus undoubtedly belongs to the pTol-DAB-centered radical of $Mn(CO)_3$(pTol-DAB), formed in the metal–metal bond splitting of **2d**. This radical is therefore better described as $^+Mn(CO)_3$(pTol-DAB)$^{\bullet-}$.

From this it can be concluded that the differences in reactivity between **1a–c** and **1d,e** are caused by the rapid thermal decomposition of **2d,e**. The instability of the latter dimers is probably caused by the better π-accepting properties of the α-diimine ligand, which induces a net electron shift from the metal d orbitals with a concomitant weakening of the metal–metal bond.

Reactions at T < 183 K. When the temperature was further lowered, the homolysis products, described in the preceding sections, were not formed anymore. Instead, irradiation with visible light of a solution of **1** in 2-MeTHF or toluene at T < 183 K, gave rise to release of CO (ν(CO) = 2132 cm^{-1}) and to the formation of a CO-loss product **7**. This reaction (5) has been

$$(CO)_5MnMn(CO)_3(\alpha\text{-diimine}) \xrightarrow{h\nu/T<183K} (CO)_4Mn(\mu\text{-CO})Mn(CO)_2(\alpha\text{-diimine}) + CO \quad (5)$$

studied in detail for the complexes **1a–c**, and the CO-stretching

Table XI. CO Stretching Frequencies and Absorption Maxima for **7a–c**

complex	ν(CO), cm^{-1}						λ_{max}^{MLCT}, nm
7a[a]	2039 m	1963 w	1939 s	1922 m	1874 m	1816 m	602
7a[b]	2041	1968	1941	1927	1875	1819	654
7b[a]	2041	1967	1947	1927	1879	1821	730
7c[a]	2034	1961	1942	1930	*c*	1824	734

[a] In 2-MeTHF; 133K. [b] In toluene; 178.5 K. [c] Obscured by bands from $Mn(CO)_5^-$.

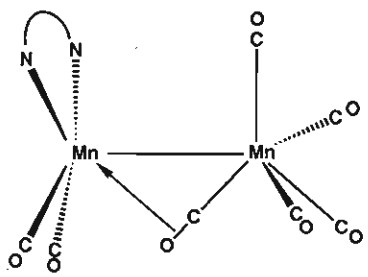

Figure 5. Schematic molecular structure of **7**.

(28) Staal, L. H.; Polm, L. H.; Balk, R. W.; van Koten, G.; Vrieze, K. *Inorg. Chem.* **1980**, *19*, 3343. Polm, L. H.; Elsevier, C. J.; van Koten, G.; Ernsting, J. M.; Stufkens, D. J.; Vrieze, K.; Andréa, R. R.; Stam, C. H. *Organometallics* **1987**, *6*, 1096.

(29) Franz, K. D. Ph.D. Thesis, Universität Frankfurt am Main, Frankfurt am Main, Germany, 1974.

frequencies together with λ_{max} of the MLCT bands of **7a–c** are collected in Table XI. The proposed structure of these photoproducts, depicted in Figure 5, is based on the following observations. The α-diimine ligand is still σ-N,σ-N′-coordinated to one metal since all complexes **7** possess an intense MLCT band in the visible region. The complexes do not contain a coordinated solvent molecule since the CO-stretching frequencies are almost the same in toluene at 178 K and in 2-MeTHF at 133 K (Table XI). The observation of a low-frequency CO band in the IR spectra of **7a–c** points to the presence of a semibridging CO ligand. An analogous product $Mn_2(CO)_9$ had been formed by irradiation of $Mn_2(CO)_{10}$ in an alkane glass.[30] In that case, however, the bridging CO ligand had a much lower frequency (ν(CO) = 1764 cm^{-1}). The competition between the formation of CO-loss and homolysis products depended on the temperature and solvent used. Both in 2-MeTHF and in toluene, 90% of **1** photoreacted with release of CO at 183 K, whereas homolysis was the only reaction observed at this temperature in CH_2Cl_2. The temperature dependence of the photoproduction of **7a–c** is certainly not due to their thermal lability but instead to a change of photoreaction. For, although **7a** is thermally stable up to 223 K, irradiation of **1a** in the temperature range 183–223 K gave rise to the formation of $Mn_2(CO)_{10}$ and coupling products of $Mn(CO)_3$(α-diimine) radicals (vide supra). The above results indicate that the influence of solvent and temperature on the photoreactions of **1** are caused by viscosity effects. In viscous media, the radicals formed by the homolysis reaction cannot diffuse and will react back to give the parent compound. The opposite effect will occur upon release of CO. The small CO molecule can escape from the solvent cage and will therefore not react back with the CO-loss product. Raising the temperature causes an increase of diffusion rate and backformation of the starting complex.

Quantum Yields. Quantum yield measurements on reaction 5 were not performed on stirred solutions by monitoring the decay of the MLCT band of **1** since irradiation at these low temperatures (T < 183 K) led to inhomogeneity within the UV cell due to the high viscosity of the solvents. Photoreactions were therefore studied for solutions in a 0.1-mm CaF_2 IR cell, the thinness of the cell minimizing sample inhomogeneities. In this way, accurate quantum yields could be determined by measuring the intensity of a carbonyl band as a function of the irradiation time t_{irr}. Mixtures of **1a** and CCl_4 (1/100) dissolved in 2-MeTHF at 298 and 173 K, were irradiated with 546-nm light, and the intensity of the 1953-cm^{-1} CO band of **1a**, $I[\nu(CO)_{1953}(t_{irr})]$, was followed during the experiment. At 173 K the solution reacted according to reaction 5; at 298 K irradiation of the reaction mixture produced $Mn(CO)_5Cl$ and $Mn(CO)_3$(bpy′)Cl according to reaction 6.

$$(CO)_5MnMn(CO)_3(bpy') \xrightarrow[CCl_4/2\text{-MeTHF}]{h\nu/298\ K} Mn(CO)_5Cl + Mn(CO)_3(bpy')Cl \quad (6)$$

Figure 6 shows a plot of ln $I[\nu(CO)_{1953}(t_{irr})]$ as a function of t_{irr} at both reaction temperatures. $I[\nu(CO)_{1953}(t_{irr})]$ and t_{irr} were multiplied by $1/I[\nu(CO)_{1953}(t_{irr}=0)]$ and $A_{546}(t_{irr}=0)$, respectively, to correct for the temperature dependence of the carbonyl band intensity and the 546-nm absorbance. Apparently, both reactions follow first-order kinetics, and by least-square analysis eqs 7 and 8 have been derived for ln $I[\nu(CO)_{1953}(t_{irr})] = kt_{irr} + C$, in which k represents the reaction constants k_6 of reaction 6 (eq 7, 298 K) and k_5 of reaction 5 (eq 8, 173 K), respectively.

$$\ln I[\nu(CO)_{1953}(t_{irr})] = 0.158t_{irr} + 0.017 \quad (T = 298\ K;\ r = 0.994) \quad (7)$$

$$\ln I[\nu(CO)_{1953}(t_{irr})] = 0.084t_{irr} + 0.019 \quad (T = 173\ K;\ r = 0.999) \quad (8)$$

From these equations, it follows that $k_5/k_6 = 0.47$. From the relationship $k = \phi I_\nu c_{1a}$ (I_ν = intensity of the light source) and the value $\phi_6 = 0.70$ mol/einstein for reaction 6 from Table VI, a quantum yield $\phi_5 = 0.33$ mol/einstein was derived for reaction 5 at 173 K. By use of the same procedure, the wavelength dependence of ϕ_5 was determined between 477 and 549 nm. The variation of the reaction constants in this wavelength region was within the standard deviation, which means that ϕ_5, just like ϕ_6, does not depend on λ_{irr} throughout the MLCT band.

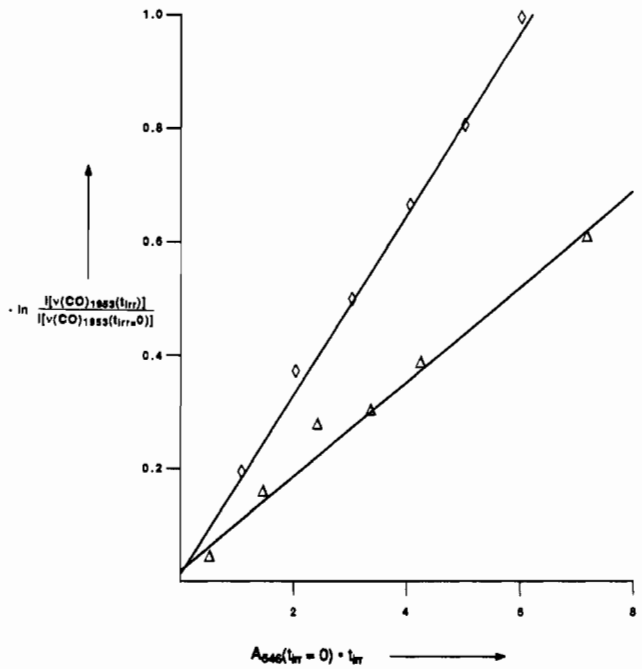

Figure 6. Normalized intensity of the 1953-cm^{-1} carbonyl band of **1a** as a function of irradiation time (λ_{irr} = 546 nm) in 2-MeTHF at 173 (Δ) and 298 K (◊).

Thermal reactions of 7a. Raising the temperature of a solution of **7a** in 2-MeTHF to 193 K caused a slow back-reaction with CO, still present in the solution, to give the parent compound. In addition, small amounts of $Mn_2(CO)_{10}$ and $Mn_2(CO)_6(bpy')_2$ were formed. When the free CO, formed during the photoproduction of **7a**, had been removed from the IR cell by bubbling cooled nitrogen through the solution, a temperature increase caused the formation of $Mn(CO)_5^-$ and of a product having CO bands at 1927 and 1842 cm^{-1}. These latter frequencies are assigned to $[Mn(CO)_2(bpy')(2\text{-MeTHF})_2]^+$ because of their close similarity with the values obtained for $[Mn(CO)_2(bpy)(PEt_3)_2]^+$.[31] We observe that 193 K seems to be about the temperature at which the CO-bridge bond is broken since the thermal reactions of **7a** with other ligands also proceeded above this temperature. These latter reactions, performed with ether, acetonitrile, *tert*-butyl isocyanide and four phosphines, gave rise to the formation of new products **8a**. Their CO-stretching frequencies closely resemble those of **7a** with the exception of the 1816-cm^{-1} band, which shifts appreciably to higher wavenumbers (Table XII). Apparently, the CO bridge has regained its terminal position in **8a**, and the substituting ligand now occupies the open site in the $Mn(CO)_2$(bpy′) fragment. The complexes **8a** are therefore formulated as $(CO)_5MnMn(CO)_2(bpy')L$ (L = CH_3CN, py, PR_3, tBuNC). Only in the case of ether did no reaction seem to have taken place since the product still contains a semibridging CO-ligand. The thermal reaction of **7a** with CCl_4 in 2-MeTHF gave rise to the formation of $Mn(CO)_4$(2-MeTHF)Cl, which means that **7a** not only takes up two electron donors but also gives rise to radical coupling reactions. During this reaction with CCl_4, the bpy′ metal fragment did not produce a stable CO-containing complex. This is, however, not surprising in view of the fact that complexes such as $Mn(CO)_3(py)_3^+$ and $Mn(CO)_3$(3,5-di-tBu-1,2-benzosemiquinone)(THF) decompose immediately into the Mn^{II} ions $Mn(py)_6^{2+}$ and Mn^{II}_4(3,5-di-tBu-1,2-benzosemiquinone)$_8$, respectively.[32,33]

(30) Hepp, A. F.; Wrighton, M. S. *J. Am. Chem. Soc.* **1983**, *105*, 5934.

(31) Usón, R.; Riera, V.; Gimeno, J.; Laguna, M. *Transition Met. Chem. (Weinheim, Ger.)* **1977**, *2*, 123.

Table XII. CO Stretching Frequencies and Absorption Maxima for **8a**(L) in 2-MeTHF at 203 K

complex	ν(CO), cm^{-1}						λ_{max}^{MLCT}, nm
7a[a]	2036 m	1957 w	1934 s	1919 m	1877 m	1817 m	660
8a(py)	2035	1958	1936	1923	1885	1827	643
8a(CH_3CN)	2037	1959	1937	1923	1895	1839	612
8a($P(nBu)_3$)	2033	1960	1948	1924	1888	1831	643
8a(PPh_3)	2036	1964	1945	1929	1892	1838	620
8a($P(OPh)_3$)	2041	1968	1947	1933	1917	1865	556
8a (tBuNC)	2032	1960	1941	1927	1907	1863	556
1a	2053 m	1979 s	1952 s		1895 m		516

[a] In the presence of ether.

Scheme III

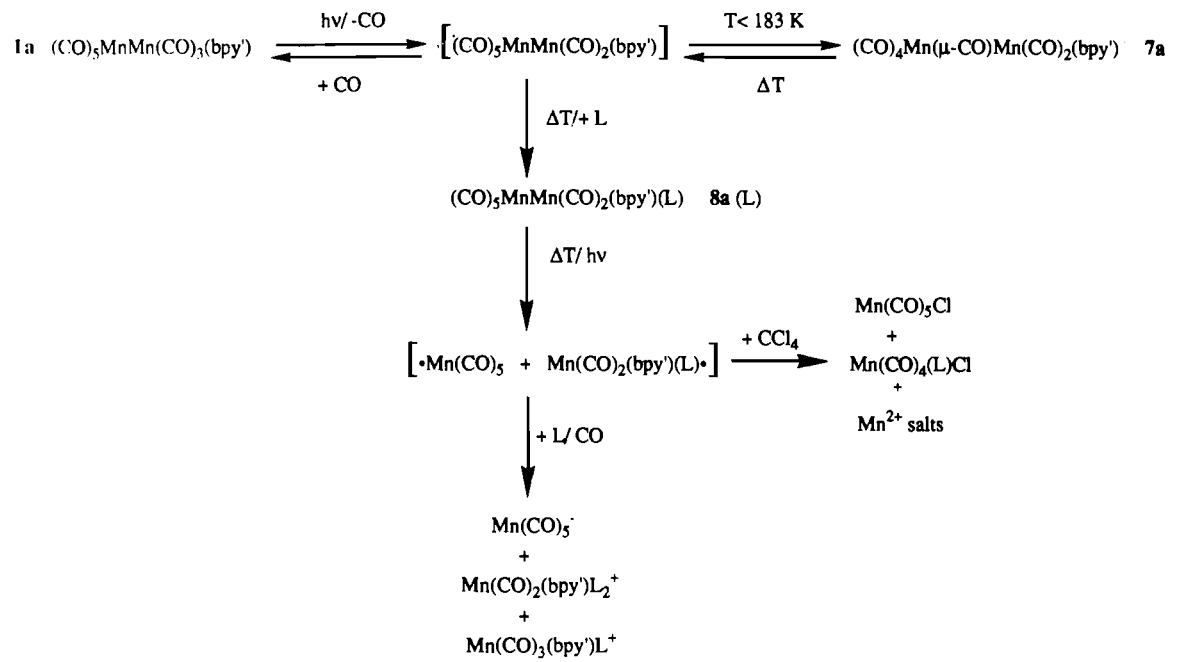

Raising the temperature of a **7a**/PPh_3/CCl_4 (1/50/50) mixture in 2-MeTHF afforded the substituted compound **8a**(PPh_3) as well as $Mn(CO)_4(PPh_3)Cl$. The suppression of the $Mn(CO)_4$(2-MeTHF)Cl formation by addition of PPh_3 was also observed in the corresponding reactions of $Mn_2(CO)_{10}$. Thus irradiation of $Mn_2(CO)_{10}/CCl_4$ (1/50) and $Mn_2(CO)_{10}/PPh_3/CCl_4$ (1/50/50) mixtures in 2-MeTHF at 193 K with the unresolved 351/364-nm lines of an argon ion laser afforded, in addition to $Mn(CO)_5Cl$, $Mn(CO)_4$(2-MeTHF)Cl and $Mn(CO)_4(PPh_3)Cl$, respectively. Interestingly, the composition of the product mixture from the thermal **7a**/PPh_3/CCl_4 reactions depended on the PPh_3 concentration, addition of more PPh_3 resulting in an increase of the ratio **8a**(PPh_3)/$Mn(CO)_4(PPh_3)Cl$.

These thermal reactions of **7a**, together with the photoreactions of **7a** and **8a**(L) (vide infra), are schematically depicted in Scheme III.

Photochemical reactions of 7a and 8a(L). Irradiation into the MLCT band of **7a** at 133 K gave rise to a slow photodisproportionation ($\phi \cong 10^{-2}$ mol/einstein) with formation of $[Mn(CO)_2(bpy')(2\text{-MeTHF})_2]^+$ and $Mn(CO)_5^-$. This photoreaction was quenched by addition of CCl_4. In the presence of PPh_3 complex **8a**(PPh_3) produced, apart from $Mn(CO)_5^-$, a mixture of $[Mn(CO)_2(bpy')(PPh_3)_2]^+$ and $[Mn(CO)_3(bpy')(PPh_3)]^+$, whereas in the case of **8a**(CH_3CN) only $[Mn(CO)_3(bpy')(CH_3CN)]^+$ was formed.

Mechanistic Aspects. The complexes under study show release of CO and homolysis of the metal–metal bond. From these reactions, CO loss is clearly not a secondary thermal process involving the homolysis products since it is not quenched by addition of the radical scavenger CCl_4. Both reactions are primary photoprocesses, and their quantum yields are high and wavelength independent throughout the MLCT band.

Similar results have recently been obtained by us for the closely related complexes $L'_mM'M(CO)_3(\alpha\text{-diimine})$ (L'_mM' = $(CO)_5Re$, $(CO)_5Mn$, $(CO)_4Co$, $CpFe(CO)_2$, Ph_3Sn),[8] and just as for these latter compounds, both reactions of **1** most probably occur from the repulsive $^3\sigma_b\sigma^*$ state after intersystem crossing/internal conversion from the MLCT state(s). The potential energy curves of the excited states involved in these reactions are schematically depicted in Figure 7. Although population of the $^3\sigma_b\sigma^*$ state will mainly weaken the metal–metal bond, the actual reaction that takes place will of course depend on the relative strengths of the metal–metal and metal–CO bonds in this state. Therefore, all $L'_mM'Re(CO)_3(\alpha\text{-diimine})$ complexes only show homolysis due to their strong Re–CO bonds. Since the Mn–CO bonds are normally much weaker,[34] the corresponding $L'_mM'Mn(CO)_3(\alpha\text{-diimine})$ complexes undergo release of CO, either in combination with homolysis (complexes **1**) or as virtually the only photoprocess ($L'_mM'Mn(CO)_3(\alpha\text{-diimine})$; L'_mM' = $(CO)_5Re$,[9] Ph_3Sn[7c]). The complexes $(CO)_4CoMn(CO)_3(\alpha\text{-diimine})$ are exceptional in showing only homolytic cleavage of the Co–Mn bond.[5]

An important property of these complexes is that none of them shows release of CO from the unsubstituted metal fragment upon MLCT excitation. Thus, the complexes $(CO)_5MnRe(CO)_3(\alpha\text{-diimine})$ only undergo homolysis although the Mn–CO bonds of the $Mn(CO)_5$ fragment are rather weak and the Mn–Re and

(32) McCullen, S. B.; Brown, T. L. *Inorg. Chem.* **1981**, *20*, 3528.
(33) Lynch, M. W.; Hendrickson, D. N.; Fitzgerald, B. J.; Pierpont, C. G. *J. Am. Chem. Soc.* **1984**, *106*, 2041.
(34) Svec, H. J.; Junk, G. A. *J. Am. Chem. Soc.* **1967**, *89*, 2836.

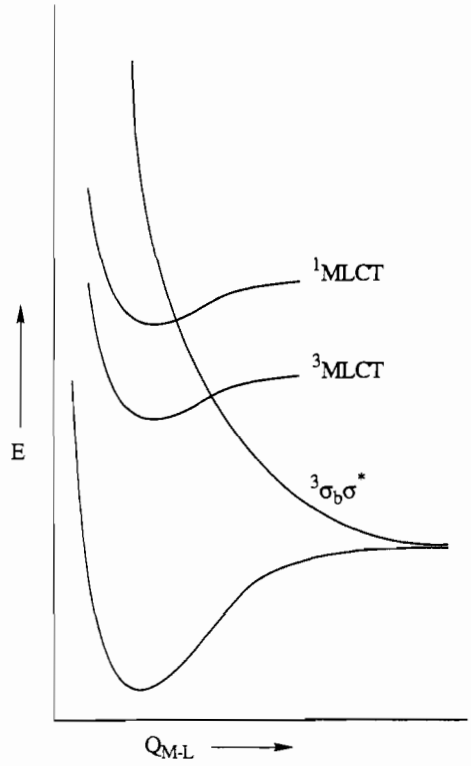

Figure 7. Schematic energy diagram for metal-metal bonded carbonyl compounds with low-lying ^{1,3}MLCT states.

Re–CO bonds strong. This means that the $^3\sigma_b\sigma^*$ state of the α-diimine derivative is confined to the M′–M(CO)$_3$(α-diimine) moiety.

Unfortunately, there is only a small (low) temperature range in which both reactions could be observed simultaneously. Because of this, it was not possible to investigate whether the quantum yields of these two reactions depend on each other. In this article, two reactions of the radicals are reported that have not been mentioned before in the literature. Although $Mn_2(CO)_{10}$ and Mn(CO)$_3$(α-diimine) radicals were shown to react with each other to give the parent compound (CO)$_5$MnMn(CO)$_3$(α-diimine) (vide supra), the Mn(CO)$_5$ and Mn(CO)$_3$(α-diimine) radicals formed out of the R-pyca (**1b**) and R-DAB (**1c–e**) complexes, produced **3b** and **4c–e**, respectively, according to Scheme I.

From the production of these latter complexes, the mechanism of the radical coupling reaction becomes clear. After homolysis, the unpaired electron of the Mn(CO)$_3$(α-diimine) radical moves to the α-diimine ligand, which has a lower (π^*) orbital than the metal center (d_{z^2}). As a result, the radicals can not react anymore with each other via a metal–metal coupling reaction, but instead they react, especially in viscous solvents or matrices, by attack of the negatively charged α-diimine ligand from the radical anion $^+$Mn(CO)$_3$(α-diimine)$^{\bullet-}$ on the metal center of the Mn(CO)$_5$ radical. In the case of the bpy′ complex, this coupling reaction will only give rise to back-formation of complex **1a**. For **1b–c**, a CN bond of the R-pyca or R-DAB ligand will instead bind to the metal with a concomitant loss of CO, thus preventing the back-formation of the starting complex. So, the complexes **3b** and **4c–e** are formed by reaction of the Mn(CO)$_5$ and Mn(CO)$_3$(α-diimine) radicals in the solvent cage, directly after their formation. This also explains why the radical scavenger CCl_4 only suppresses the formation of these complexes at rather high concentrations (vide supra).

The dimerization of the Mn(CO)$_3$(R-DAB) radicals, shown in Scheme II, is also a remarkable reaction. Again, no direct metal–metal coupling reaction occurs. Instead, the radical anions of the 16-electron zwitterionic radical complexes $^+$Mn(CO)$_3$(α-diimine)$^{\bullet-}$ (ESR[19b]) will attack the coordinatively unsaturated and positively charged metal center of their counterparts. For the bpy′ radicals, this interaction will only give rise to charge transfer and metal–metal bond formation; in the case of the iPr-DAB radicals, these reactions are followed by metal–CN bond formation and release of CO.

Finally, we would like to make a short remark concerning the low-temperature photodisproportionation of **7a** and **8a**(L′). This reaction is quenched by CCl_4, which means that the primary photoprocess is homolysis. Irradiation of **7a** in 2-MeTHF produces the 14-electron radical complex Mn(CO)$_2$(bpy′), which will take up two solvent molecules. The Mn(CO)$_2$(bpy′)(2-MeTHF)$_2$ radicals, thus formed, are highly reducing species that will transfer an electron to the Mn(CO)$_5$ radicals and to the parent compound. This explains the formation of [Mn(CO)$_2$(bpy′)(2-MeTHF)$_2$]$^+$ and Mn(CO)$_5^-$. In the case of **8a**(L′) homolysis produces Mn(CO)$_5$ and Mn(CO)$_2$(bpy′)(L′). Depending on the coordinating properties of L′, the Mn(CO)$_2$(bpy′)(L′) radical will react further with L′ to give Mn(CO)$_2$(bpy′)(L′)$_2$ or produce Mn(CO)$_3$(bpy′)L′ by reaction with CO still present in the solution. Both types of radicals will undergo an electron-transfer reaction.

Conclusion

The complexes under study photoreact with homolysis of the metal–metal bond and release of CO, most probably from the same repulsive $^3\sigma_b\sigma^*$ state. The radicals formed by the homolysis reaction undergo different coupling reactions. In the case of the R-pyca and R-DAB complexes, these reactions can lead to the formation of interesting coupling products that present evidence for the reaction mechanisms.

Acknowledgment. We thank Prof. Dr. W. Kaim for a helpful discussion of the ESR spectra and the Netherlands Foundation for Chemical Research (SON) and the Netherlands Organisation for the Advancement of Pure Research (NWO) for their financial support.

Supplementary Material Available: Listings of the atomic coordinates (Table S1), the anisotropic thermal parameters for non-hydrogen atoms and isotropic thermal parameters for hydrogen atoms (Table S2), and all nonessential bond lengths and angles (Table S3) (4 pages); a listing of structure factor amplitudes (Table S4) (20 pages). Ordering information is given on any current masthead page.